Acta Cryst. (1998). D**54**, 834–843

X-ray Structure of Human Lysozyme Labelled with 2′,3′-Epoxypropyl β-Glycoside of Man-β1,4-GlcNAc. Structural Change and Recognition Specificity at Subsite *B*

MICHIRO MURAKI,[a]* KAZUAKI HARATA,[a] NAOKI SUGITA[b] AND KEN-ICHI SATO[b]

[a]*Biomolecules Department, National Institute of Bioscience and Human Technology, Tsukuba, Ibaraki 305, Japan, and* [b]*Faculty of Engineering, Kanagawa University, Yokohama, Kanagawa 221, Japan. E-mail: muraki@nibh.go.jp*

(*Received 11 June 1997; accepted 19 January 1998*)

Abstract

Human lysozyme (HL) labelled with the 2′,3′-epoxypropyl β-glycoside of Man-β1,4-GlcNAc was crystallized at pH 4.5. The cell dimensions were $a = 36.39$, $b = 116.38$, $c = 30.91$ Å and the space group was $P2_12_12_1$. The unit cell contained four molecules ($V_m = 2.18$ Å^3 Da^{-1}). The crystal structure was determined by molecular replacement and refined to an R value of 0.168 for 7060 reflections [$|F_o| > 3\sigma(F)$] in the resolution range 8.0–2.1 Å. A prominent shift of the C^α-atom positions by up to 3.8 Å in the region of residues 45–50 was observed compared with wild-type HL. Owing to the conformational change in this region the intermolecular contacts were altered remarkably compared with wild-type HL, explaining the difference in molecular packing. The Man-β1,4-GlcNAc moiety occupied subsites *B* and *C* in the substrate-binding site of HL. Several differences in the hydrogen-bonded contacts between the ligand part and the protein part were observed for HL labelled with the 2′,3′-epoxypropyl β-glycoside of Man-β1,4-GlcNAc compared with HL labelled with the corresponding derivatives of GlcNAc-β1,4-GlcNAc and Gal-β1,4-GlcNAc. In contrast to the replacement of GlcNAc with Gal, the replacement of GlcNAc with Man did not sacrifice the stacking interactions with the side-chain group of Tyr63 as determined by the parallelism of the apolar face of the carbohydrate residue and the aromatic plane of the Tyr63 side chain. The 2′,3′-epoxypropyl β-glycoside of Man-β1,4-GlcNAc exhibited almost the same affinity towards HL as Gal-β1,4-GlcNAc, a much lower affinity than that of GlcNAc-β1,4-GlcNAc. The difference in the protein–ligand interactions was discussed in relation to the carbohydrate-residue recognition specificity at subsite *B* of HL. The results suggested that Gln104 was a determinant for the strong recognition of GlcNAc residue at subsite *B* in HL.

1. Introduction

Sequence-specific recognition of polysaccharides by carbohydrate-binding proteins plays a crucial role in many important biological processes for the maintenance of homeostasis of living animals and plants (Quiocho, 1986). This includes the recognition of bacterial cell-wall polysaccharide by human lysozyme, one of the c-type lysozymes. The first observation of saccharide binding in the active site of a c-type lysozyme was reported by Blake *et al.* (1967). Since then, the interaction mode between c-type lysozymes and saccharide sequences has been studied by many investigators in atomic detail using X-ray crystallography. For example, the interaction of MurNAc-GlcNAc-MurNAc (Strynadka & James, 1991) or $(GlcNAc)_3$ (Cheetham *et al.*, 1992) with hen egg-white lysozyme (HEWL) and the interaction of $(GlcNAc)_4$ plus $(GlcNAc)_2$ with HL (Song *et al.*, 1994) have been reported. The active site of c-type lysozymes, including HL, has generally been considered to be composed of six subsites designated from *A* to *F*, each of which accommodate a monomeric carbohydrate residue. Many studies on the substrate-recognition mechanism involving subsites *B* and *C* of c-type lysozymes have been performed. However, detailed structural descriptions of interaction with disaccharide sequences other than the GlcNAc-β1,4-GlcNAc or MurNAc-β1,4-GlcNAc sequences at these subsites are few.

Since the physiological role of lysozyme has not yet been completely clarified (Jollès & Jollès, 1984), the possible interaction of lysozyme with other saccharide sequences existing in biological sources is biochemically worth probing. The Man-β1,4-GlcNAc sequence is ubiquitously found in the core structure of *N*-linked oligosaccharides of glycoproteins and also found in carbohydrate-storage materials from some patients with conditions such as mannosidosis, as a disaccharide component (Dawson, 1978). Affinity labelling of hen egg-white lysozyme by 2′,3′-epoxypropyl β-glycoside derivatives of GlcNAc oligomers was reported by Thomas *et al.* (1969), and the attachment site of the labelling reagent has been identified (Moult *et al.*, 1973). In a previous paper, we revealed the interaction mode between HL and Gal-β1,4-GlcNAc by affinity labelling (Muraki *et al.*, 1996). We describe here the interaction mode between c-type lysozyme and Man-β1,4-GlcNAc for the first time, as probed by means of affinity labelling. X-ray structural analysis revealed a change in the

ISSN 0907-4449

main-chain conformation induced by the attachment of the labelling reagent. The structural comparison of HL labelled with the 2′,3′-epoxypropyl β-glycoside derivative of Man-β1,4-GlcNAc (the HL/MAN–NAG–EPO complex), HL labelled with the 2′,3′-epoxypropyl β-glycoside derivative of GlcNAc-β1,4-GlcNAc (the HL/NAG–NAG–EPO complex) and HL labelled with the 2′,3′-epoxypropyl β-glycoside derivative of Gal-β1,4-GlcNAc (the HL/GAL–NAG–EPO complex) have provided information on the carbohydrate-residue recognition specificity at subsite *B* of HL.

2. Materials and methods

2.1. *Materials*

The affinity-labelling reagent, the 2′,3′-epoxypropyl β-glycoside of Man-β1,4-GlcNAc, was synthesized organo-chemically, according to the methods of Sato *et al.* (1997) and Thomas (1970). *N*-acetyllactosamine was used as the starting material for the synthesis. The product was a mixture of the (2*R*) and the (2*S*) stereoisomers at the epoxide group. ^{1}H NMR analysis showed the sample to be essentially pure. The ratio of the stereoisomers was 4:1, with the same stereoisomer in excess as in the cases of the labelling reagents GlcNAc-β1,4-GlcNAc and Gal-β1,4-GlcNAc (Muraki *et al.*, 1996). All other reagents were analytical or biochemical grade.

2.2. *Crystallization and structure determination*

HL (20 mg) and the 2′,3′-epoxypropyl β-glycoside of Man-β1,4-GlcNAc (30 mg) were incubated in 1.5 ml of 0.2 *M* sodium acetate buffer (pH 5.4) at 310 K. After the reaction had proceeded until the reaction mixture showed less than 1% of the initial lytic activity, the reaction mixture was separated by cation-exchange chromatography (Mono S, Pharmacia). The main peak, detected at 280 nm, contained the affinity-labelled HL. The crystallization conditions were essentially the same as for wild-type HL, the HL/NAG–NAG–EPO complex and the HL/GAL–NAG–EPO complex. 5 *M* ammonium nitrate at pH 4.5 was used as the precipitant (Muraki *et al.*, 1991). Similarly shaped prisms as observed for the HL/NAG–NAG–EPO complex appeared. The space group ($P2_12_12_1$) of the crystals of the HL/MAN–NAG–EPO complex was the same as that of wild-type HL, the HL/NAG–NAG–EPO complex and the HL/GAL–NAG–EPO complex. However, the cell constants of the HL/MAN–NAG–EPO complex (Table 1) were quite different from the other complexes (Muraki *et al.*, 1996). The diffraction data collection was carried out by an automated oscillation-camera system, R-AXIS IIc (Rigaku), equipped with an imaging-plate detector. Cu $K\alpha$ radiation focused by a double-mirror system was generated using a Rotaflex FR rotating-anode generator operated at 1.6 kW (40 kV × 40 mA). The data were processed with the R-AXIS IIc data-processing software

Table 1. *Data-collection statistics and refinement parameters*

Data collection	
Space group†	$P2_12_12_1$ ($P2_12_12_1$)
Cell dimensions (Å)†	
a	36.39 (57.14)
b	116.38 (61.02)
c	30.91 (33.10)
Resolution range (Å)	36.4–2.07
Number of measured reflections	22724
Number of unique reflections	7438
R_{merge} (%)	5.7
Completeness of data (%)	94.9
Refinement	
Resolution range (Å)	8.0–2.1
Number of reflections used ($\|F\| > 3\sigma F$)	7060
R factor (%)	16.8
Free *R* factor (%)	24.8
R.m.s. deviations from ideality	
Bond lengths (Å)	0.011
Bond angles (°)	1.637

† Values for wild-type HL are in parentheses.

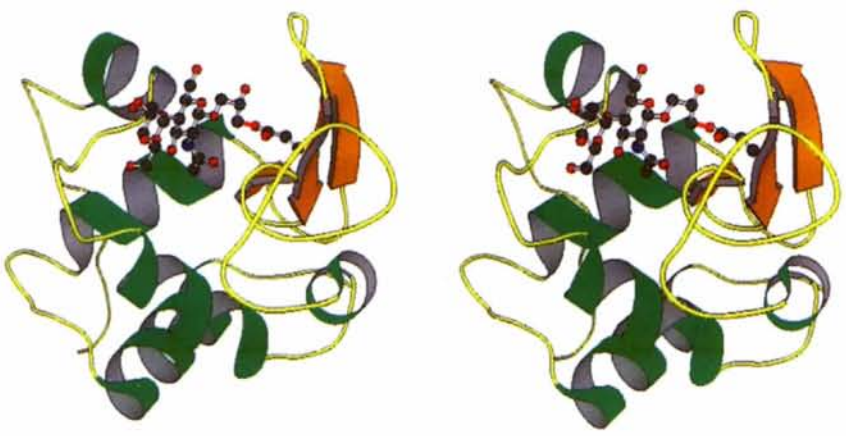

Fig. 1. Stereoview of the structure of the HL/MAN–NAG–EPO complex. The ligand part and the Asp53 side chain are shown as ball-and-stick models. The covalent bond which connects the ligand and Asp53 is drawn as a thick red line.

Table 2. *Some stereochemical parameters of disaccharides*

φ and ψ are the torsion angles about C1—O1(O4′) and O1(O4′)—C4, defined by O5—C1—O1(O4′)—C4′ and C1—O1(O4′)—C4′—C5′, respectively. ψ_H is the helical twist parameter, defined as the average of the pseudorotation angles ψ_1 = O5—C1—C4′—C3′ and ψ_2 = C2—C1—C4′—C5′ (Mo & Jensen, 1978).

Linkage	φ (°)	ψ (°)	ψ_H (°)	O5—O3′ (Å)	C6—O6 bond†	
					131	132
MAN131–NAG132	−96	−123	20	3.1	(−)-*gauche*	(+)-*gauche*
NAG131–NAG132‡	−84	−120	35	3.0	(−)-*gauche*	(+)-*gauche*
GAL131–NAG132‡	−69	−119	53	3.0	*trans*	(+)-*gauche*

† Conformation in relation to the C5—O5 bond. ‡ Values are those in the structure determined by Muraki *et al.* (1996).

package (Sato *et al.*, 1992). The structure determination of the HL/MAN–NAG–EPO complex was accomplished by a molecular-replacement method using *X-PLOR version* 3.1 (Brünger *et al.*, 1987). A modified set of coordinates of the HL/NAG–NAG–EPO complex (Protein Data Bank, entry code 1REY), which lacked the coordinates for the GlcNAc131 residue, was used as the starting model. The number of protein molecules in an asymmetric unit was one, judging by the V_m value (2.18 Å^3 Da^{-1}). The cross-rotation search was performed using Patterson vectors in the range 15.0–4.0 Å. The 180 solutions obtained were subjected to a PC refinement, which gave a single plausible solution. The translation search was performed using 15.0–4.0 Å data. The rigid-body refinement for the solution with the highest correlation (12.6σ above the mean value) gave an R value of 0.345 for 8.0–2.1 Å data. At this stage the $(F_o - F_c)$ difference map clearly showed the electron density of the mannose residue. The model could be fitted to the density very well. The model was further refined by a simulated-annealing method using *X-PLOR*. Water molecules which could form at least one hydrogen bond with a protein atom or with an already existing water molecule were included only if the final B factor was less than 60 Å^2. The coordinate error was estimated to be less than 0.25 Å using the method of Luzzati (1952). All stereochemical parameters of the final model checked by *PROCHECK* (Laskowski *et al.*, 1993) were either within or better than the average value ranges obtained from good-quality models. Some data-collection statistics and refinement parameters are summarized in Table 1. All graphical drawings of three-dimensional structures were produced using *MOLSCRIPT* (Kraulis, 1991) and *TURBO-FRODO* (Jones, 1978). The coordinates and structure factors have been deposited with the Protein Data Bank (Bernstein *et al.*, 1977). †

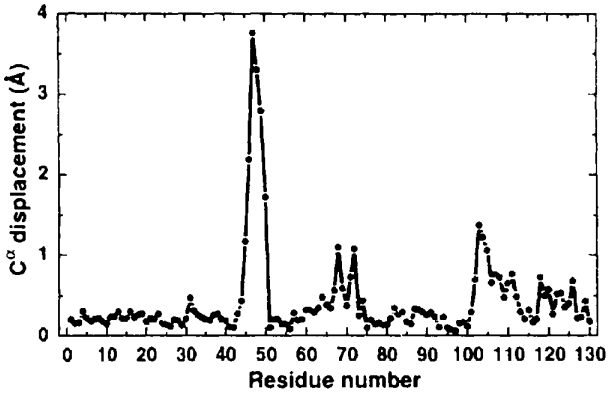

Fig. 2. Plot of the positional shifts of equivalent Cα atoms of the HL/MAN–NAG–EPO complex from wild-type HL. The shift values are calculated after least-squares fitting of the main-chain atoms.

2.3. *Reaction of HL with affinity-labelling reagent*

The experiment to follow the time-dependent inactivation has been carried out as described (Muraki *et al.*, 1996) with the exception that HL (1.0×10^{-5} M) was incubated with an affinity-labelling reagent (6.6×10^{-3} M) in 0.2 M sodium acetate buffer (pH 5.4) at 310 K.

3. Results and discussion

3.1. *Structure of the protein part*

The least-squares superposition showed that the overall main-chain structure of the HL/MAN–NAG–EPO complex (Fig. 1) was very similar to that of wild-type HL. The average displacement value of the main-chain atoms was 0.43 Å. However, as shown in Fig. 2, significant shifts of Cα atoms were observed in several regions. The most prominent shift (maximum 3.8 Å) was observed in the region containing residues 45–50. Shifts in the region containing residues 67–72 (maximum 1.1 Å) and in the region containing residues 102–112 (maximum 1.4 Å) were also observed. The conformational change in the main-chain structure of these regions is presented in Fig. 3. For further estimation of the structural change induced by ligand binding, the difference-distance maps of all Cα atoms against wild-type HL were calculated for the HL/MAN–NAG–EPO and HL/NAG–NAG–EPO complexes (Fig. 4). A short loop region of residues 45–50, connecting two β-strands, moved significantly closer (by a maximum of 4.0 Å) towards all regions except residues 67–72 (Fig. 4*a*),

† Atomic coordinates and structure factors have been deposited with the Protein Data Bank, Brookhaven National Laboratory (Reference: 1REM).

Table 3. *Comparison of possible carbohydrate–protein hydrogen bonds in the HL/MAN–NAG–EPO, HL/NAG–NAG–EPO and HL/GAL–NAG–EPO complexes*

Only bonds of less than 3.3 Å are included.

Subsite	Carbohydrate atom	Protein atom	Distance (Å)† HL/MAN–NAG–EPO	HL/NAG–NAG–EPO‡	HL/GAL–NAG–EPO‡
B	O2	Gln 104 OE1	3.2	–	–
	N2	Tyr63 OH	–	2.8/2.8	–
	O3	Gln104 N	–	–	2.9/3.3
	O4	Asp102 OD1	–	–	2.7
	O4	Gln104 NE2	–	–	3.1/2.9
	O4	Gln104 N	–	–	2.9/2.8
	O5	Gln104 NE2	2.8	2.9/2.7	3.1/2.9
	O6	Asp102 OD1	2.6	2.6	–
	O6	Gln104 NE2	2.8	2.7/2.7	–
	O6	Gln104 N	3.1/2.9	–	–
	O7	Gln104 NE2	–	3.3	–
C	N2	Ala108 O	2.7	3.0	2.9
	O3	Trp64 NE1	3.1	3.2	3.2
	O3	Gln104 NE2	3.2	–	–
	O4	Gln104 NE2	–	3.1	–
	O7	Asn60 N	2.8	2.9	3.0

† The distances of water-mediated hydrogen bonds are shown as the distances of (sugar atom–water atom)/(water atom–protein atom). Water–water bridge mediated hydrogen bonds are excluded. ‡ Values are those in the structure determined by Muraki *et al.* (1996).

which correspond to the adjacent large loop region (Fig. 3*a*). A switch of hydrogen bonds in this region occurs during the shift in atom positions. Although the precise mechanism of the conformational change is unclear, the additional formation of a type I β-turn structure consisting of Ala47, Gly48, Asp49 and Arg50

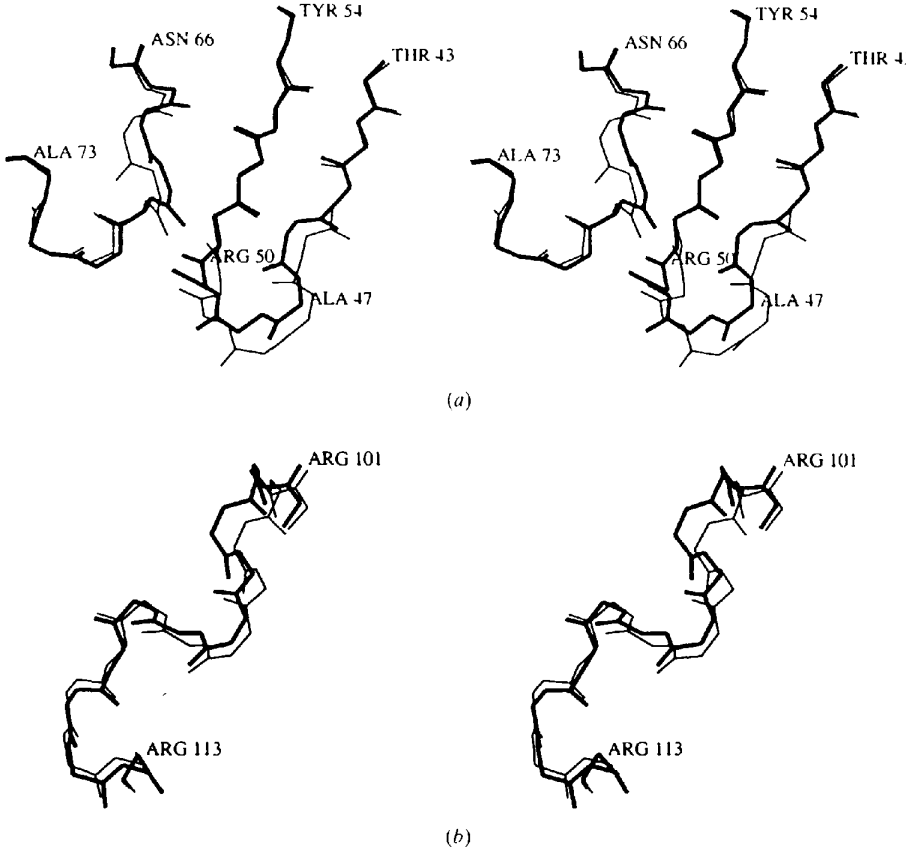

Fig. 3. Superposition of the partial main-chain structure. After the least-squares fitting of the main-chain atoms, the corresponding parts of the structures of the HL/MAN–NAG–EPO complex and wild-type HL are shown as thick lines and thin lines, respectively. (*a*) Residues 43–54 and residues 66–73, (*b*) residues 101–113.

in the HL/MAN–NAG–EPO complex may partly account for the change. The binding of the ligand made the catalytic cleft narrower. The 103rd residue centred region moved toward the regions of residues 42–54 and residues 59–80, constituting the 'left-hand side' cleft lobe of HL, during the ligand binding. This motion corresponds to an induced fit to the ligand. In the region of residues 45–50, the shift derives from the large local conformational change in the main-chain structure which takes place during the movement. However, the fitting motion itself was less distinct in the HL/MAN–NAG–EPO complex (Fig. 4*a*) compared with the HL/NAG–NAG–EPO complex (Fig. 4*b*). On the other hand, the 103rd residue centred region moved away from the regions of residues 4–30 and residues 121–130, which comprise the rear of the 'right-hand side' cleft lobe of HL. The movement was also less apparent in the binding of the 2′,3′-epoxypropyl β-glycoside of Man-β1,4-GlcNAc (MAN–NAG–EPO) ligand (maximum 1.3 Å) (Fig. 4*a*) than in the binding of the corresponding GlcNAc-β1,4-GlcNAc (NAG–NAG–EPO) ligand (maximum 2.4 Å) (Fig. 4*b*).

The region of residues 47–50 contributed significantly to the intermolecular contacts, including several intermolecular hydrogen bonds, in the molecular packing of the wild-type HL crystal structure (Fig. 5*a*). The contacts were mostly maintained in the crystals of the HL/NAG–NAG–EPO and HL/GAL–NAG–EPO complexes. In contrast, the intermolecular contacts in this region were altered remarkably in the HL/MAN–NAG–EPO complex (Fig. 5*b*) owing to the prominent shift of the main-chain structure (Fig. 2). The altered molecular packing in the unit cell (Fig. 6) explained the large differences in the cell parameters of the HL/MAN–NAG–EPO complex compared with those of wild-type HL (Table 1). The average temperature factors for each residue are plotted in Fig. 7. The average B value was 17.8 Å^2 for all main-chain atoms and 23.7 Å^2 for all side-chain atoms in the HL/MAN–NAG–EPO complex. The average B values of the main-chain atoms of residues Ala47 and Gly48 were significantly higher (33.0 and 39.5 Å^2) in the HL/MAN–NAG–EPO complex compared with those in wild-type HL (16.6 and 16.9 Å^2), the HL/NAG–NAG–EPO complex (21.9 and 23.4 Å^2) and the HL/GAL–NAG–EPO complex (16.6 and 17.4 Å^2). The absence of the intermolecular hydrogen bond in which these residues participated (Fig. 5*b*) should be responsible for the higher B values.

3.2. *Structure of the ligand part*

The omit ($F_o - F_c$) electron-density map (Fig. 8) clearly shows the bound ligand including the connection region between the protein part and the ligand part. It confirms the covalent binding of the labelling reagent to Asp53 of HL *via* an ester bond of high occupancy. The Man-β1,4-GlcNAc (MAN–NAG) moiety of the labelling reagent occupied subsites B and C in essentially the same manner as the GlcNAc-β1,4-GlcNAc (NAG–NAG) or Gal-β1,4-GlcNAc (GAL–NAG) moiety (Muraki *et al.*, 1996). Some stereochemical parameters of the ligand part in the HL/MAN–NAG–EPO, HL/NAG–NAG–EPO and HL/GAL–NAG–EPO complexes are summarized in Table 2. All pyranose

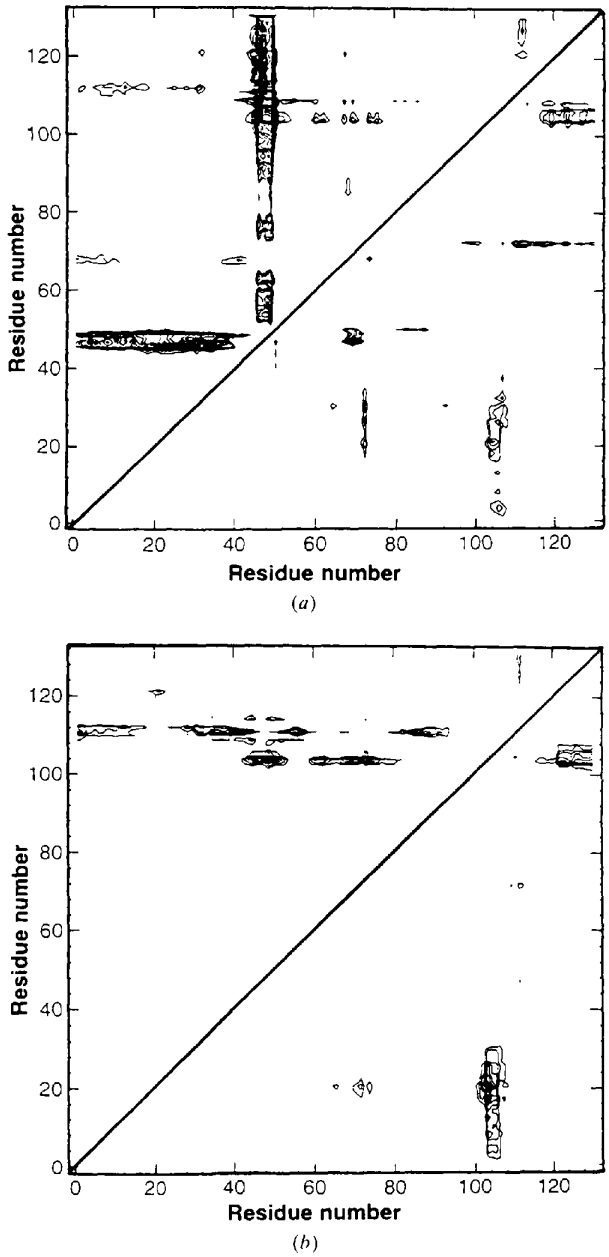

Fig. 4. Difference-distance map against wild-type HL. The difference $C^{\alpha}-C^{\alpha}$ distances, Δr_{ij} (complex) − Δr_{ij} (wild-type), are plotted. Contours are drawn at −0.6, −0.8, −1.0 *etc.* (top left) and 0.6, 0.8, 1.0 *etc.* (bottom right). (*a*) HL/MAN–NAG–EPO complex, (*b*) HL/NAG–NAG–EPO complex.

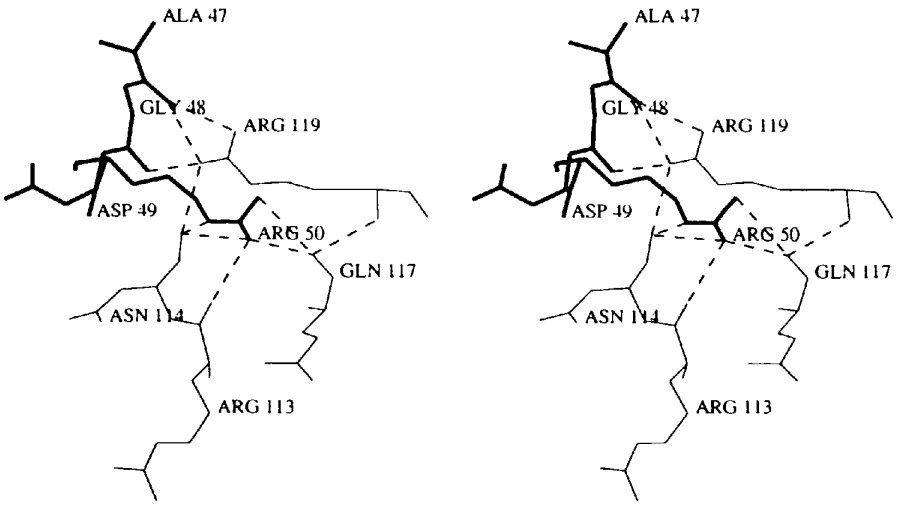

Fig. 5. Intermolecular contacts involving residues 47–50. The original molecule and symmetry-related molecule concerned are drawn with thick lines and thin lines, respectively. The broken lines denote possible hydrogen bonds. (*a*) Wild-type HL (symmetry operator, $-x + \frac{1}{2}, -y, z + \frac{1}{2}$); (*b*) HL/MAN-NAG-EPO complex (symmetry operator, $x + \frac{1}{2}, -y + \frac{1}{2}, -z$).

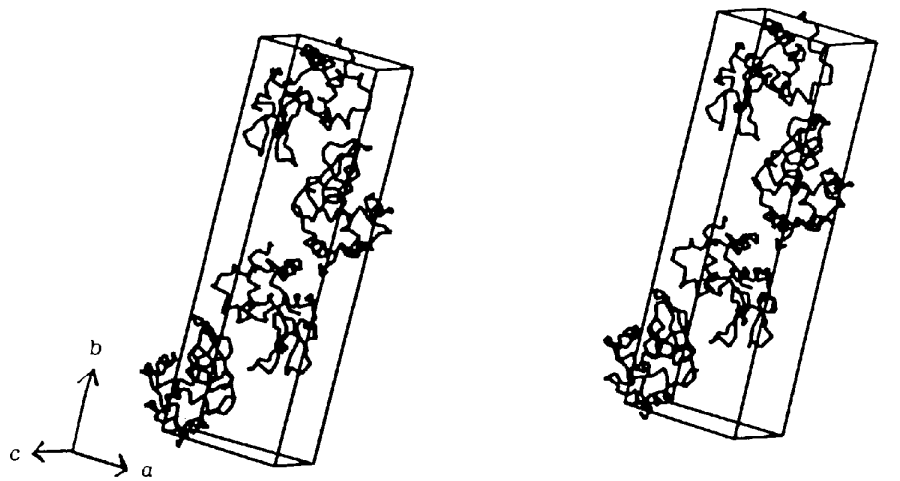

Fig. 6. Stereo drawing of crystal packing of the HL/MAN-NAG-EPO complex. A unit cell and C^{α} trace of molecules are drawn.

rings in these complexes took a normal chair conformation. The C6—O6 bond in the GlcNAc (NAG) residue occupying subsite *C* had (+)-*gauche* conformation in relation to the C5—O5 bond in all complexes. In the case of the residue occupying subsite *B*, (−)-*gauche* conformation was observed for MAN131 and NAG131, while *trans* conformation was observed for GAL131. In contrast to the case of the GAL–NAG linkage in the HL/GAL–NAG–EPO complex, a larger φ value and a smaller ψ_H value of the MAN–NAG linkage were observed in the HL/MAN–NAG–EPO complex compared with the NAG–NAG linkage in the HL/NAG–NAG–EPO complex. The average temperature factors for residues 131 and 132 were 28.2 and 16.5 Å^2 (HL/MAN–NAG–EPO complex), 31.2 and 21.4 Å^2 (HL/NAG–NAG–EPO complex) and 23.5 and 17.1 Å^2 (HL/GAL–NAG–EPO complex), respectively. These values were comparable to the average *B* values of the saccharide residues occupying subsites *B* and *C* in the HL/$(NAG)_4$–$(NAG)_2$ complex (24.3 and 19.1 Å^2) (Song *et al.*, 1994). The result suggested that covalent bond formation between the protein part and the ligand part did not essentially affect the flexibility of the saccharide residues.

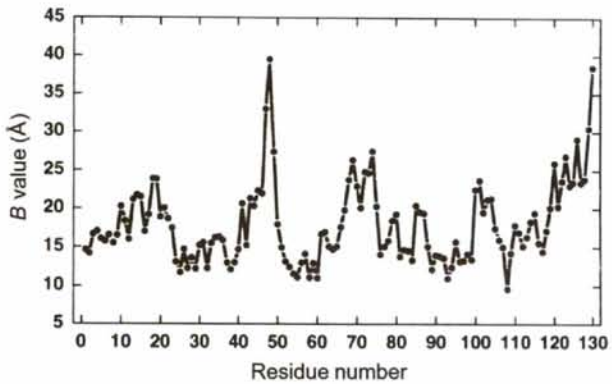

Fig. 7. Plot of average *B* values of the main-chain atoms.

3.3. *Carbohydrate–protein interaction*

The possible hydrogen-bonding network around the ligand part in the HL/MAN–NAG–EPO complex is shown schematically in Fig. 9. In Table 3, the major hydrogen-bonded contacts between the ligand part and the protein part in the HL/MAN–NAG–EPO, HL/NAG–NAG–EPO and HL/GAL–NAG–EPO complexes are summarized. Compared with the NAG131 residue at subsite *B* in the HL/NAG–NAG–EPO complex, the MAN131 residue in the HL/MAN–NAG–EPO complex has lost the direct hydrogen bond from O7 to Gln104 NE2 and the water-mediated hydrogen bond from N2 to the side-chain hydroxyl group of Tyr63, due to the lack of an equatorial 2-*N*-acetylamino group. On the other hand, the MAN131 residue gains a possible direct hydrogen bond from O2 to Gln104 OE1 and a water-mediated hydrogen bond from O6 to Gln104 N. A pair of water-mediated hydrogen bonds in the HL/NAG–NAG–EPO complex, from O5 of the NAG131 residue to Gln104 NE2 and O6 of the NAG131 residue to Gln104 NE2, were replaced with corresponding direct hydrogen bonds in the HL/MAN–NAG–EPO complex. The conformation of the C6—O6 bond in the 131st residue (Table 2) was likely to be responsible for the hydrogen-bonded contact to Asp102

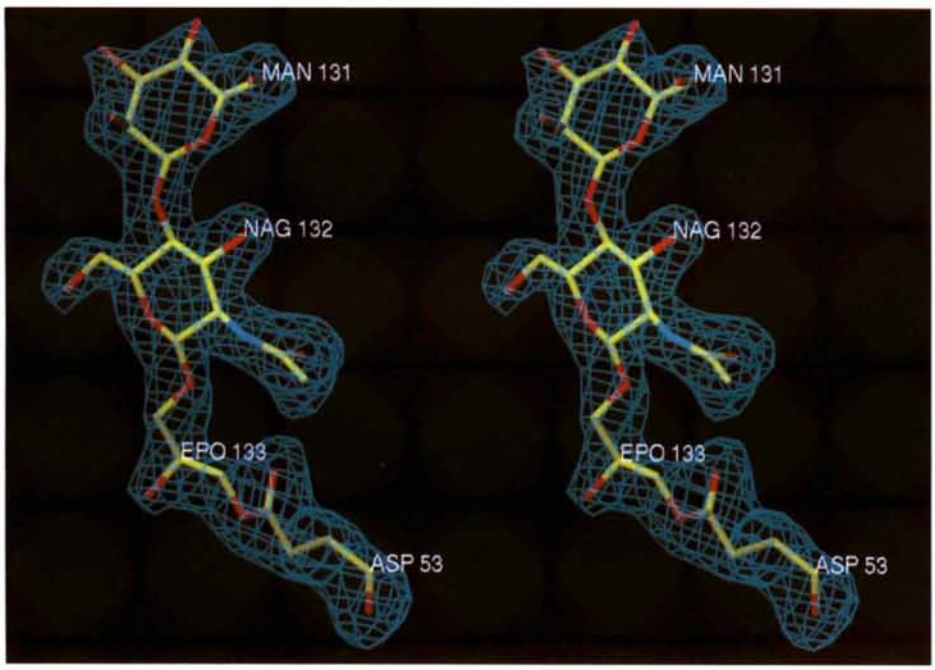

Fig. 8. Stereoview of the omit difference ($F_o - F_c$) electron-density map (contoured at 2.5σ) shown with the refined position of the ligand and Asp53 of HL superimposed.

in HL. The C6—O6 bond of the MAN131 residue in the HL/MAN–NAG–EPO complex had (−)-*gauche* conformation with respect to the C5—O5 bond, as did that of the NAG131 residue in the HL/NAG–NAG–EPO complex. For both complexes, a direct hydrogen bond between the O6 atom of the 131st residue and Asp102 OD1 was observed (Table 3). This hydrogen bond was absent in the HL/GAL–NAG–EPO complex.

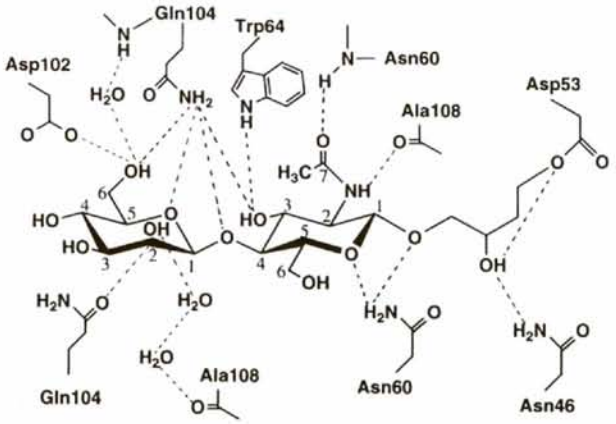

Fig. 9. Schematic drawing of the possible hydrogen-bonding interactions between the protein and ligand in the HL/MAN–NAG–EPO complex. Hydrogen-bonded contacts of less than 3.5 Å are shown with broken lines. All HL residues belong to the same molecule.

The presence of a bulky axial OH group at position 4 may make the C6—O6 bond in the GAL131 residue energetically prefer *trans* conformation to (−)-*gauche* conformation with respect to the C5—O5 bond. As shown in Table 3, the major possible hydrogen-bonded contacts at subsite *C* were almost conserved during the replacement of NAG–NAG–EPO by the corresponding derivative of MAN–NAG–EPO. However, the hydrogen bond between the O4 atom of the NAG132 residue and Gln104 NE2 in the HL/NAG–NAG–EPO complex was replaced with that between the O3 atom of the NAG132 residue and Gln104 NE2 in the HL/MAN–NAG–EPO complex.

In addition to the hydrogen-bonded contacts, the stacking of the aromatic residues against the faces of the carbohydrate residue is a distinct feature of protein–carbohydrate interactions (Vyas, 1991). Fig. 10 illustrates the geometrical relationship between Tyr63 and the carbohydrate residue at subsite *B* of HL in the HL/MAN–NAG–EPO, HL/NAG–NAG–EPO and HL/GAL–NAG–EPO complexes. In contrast to the replacement of NAG131 by GAL131 (Muraki *et al.*, 1996), the replacement of NAG131 by MAN131 did not sacrifice the stacking interaction with the side-chain group of Tyr63 in HL. Moreover, considering the parallelism of the aromatic plane of the side-chain group in the protein and the faces of the carbohydrate residue,

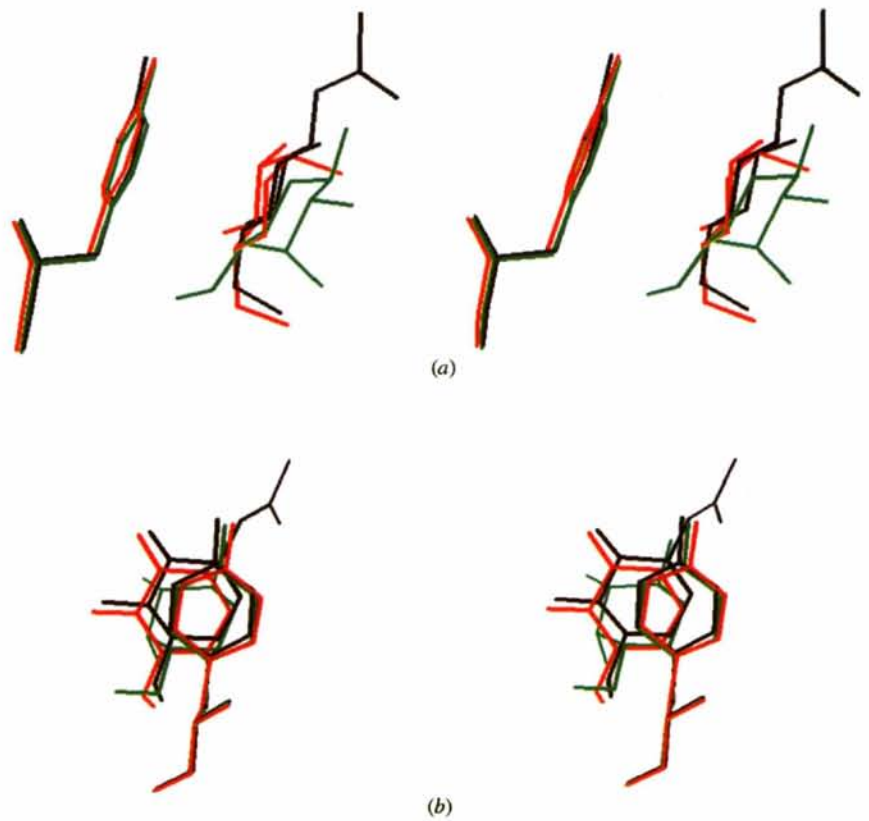

Fig. 10. Stereoview of the conformations of Tyr63 in HL and the saccharide residue at subsite *B*. After least-squares fitting of the main-chain atoms, the corresponding parts of the HL/MAN–NAG–EPO, HL/NAG–NAG–EPO and HL/GAL–NAG–EPO complexes are drawn with red, black and green lines, respectively. (*a*) Parallel view, (*b*) vertical view.

the orientation of the MAN131 residue shifts slightly to give better stacking with the phenol-ring plane of the Tyr63 side chain. The OH group at position 2 took the axial conformation in the MAN residue. This made the other side of the face more hydrophobic than the NAG residue, which possesses a hydrophilic *N*-acetylamino group at the same position in the equatorial conformation. Therefore, the stronger hydrophobic interaction might cause improved parallelism of the two faces.

3.4. *Implications for the carbohydrate recognition specificity at subsite B*

MAN–NAG–EPO inactivated HL exponentially with time, as did NAG–NAG–EPO and GAL–NAG–EPO (Fig. 11). The reaction mixture comprised 6.6×10^{-3} *M* labelling reagent and 1.0×10^{-5} *M* HL at pH 5.4 and 310 K. The reaction time required to reduce the lytic activity against *M. luteus* cells to 50% of original activity was 6.8, 13.6 and 15.0 h for NAG–NAG–EPO, GAL–NAG–EPO and MAN–NAG–EPO, respectively. This indicated that the half-life of the lytic activity was lengthened by 2.0 times and 2.2 times by the replacement of the non-reducing end-sugar residue GlcNAc by Gal and Man, respectively. Since the inactivation rates were directly affected by the strength of the association of the saccharide moieties with the lysozyme (Thomas *et al.*, 1969), the results suggested that Man-β1,4-GlcNAc possessed a much lower affinity than GlcNAc-β1,4-GlcNAc and a similar affinity to Gal-β1,4-GlcNAc.

There were several differences between the hydrogen-bonded contacts in subsite *B* in the HL/NAG–NAG–EPO and HL/MAN–NAG–EPO complexes (Table 3). Among them, the water-mediated hydrogen bond to Tyr63 seems to be unimportant, as replacement of Tyr63 with Phe did not change the K_M value for the *p*-nitrophenyl chitopentaoside significantly (Muraki *et al.*, 1992). The replacement of the two water-mediated hydrogen bonds involving Gln104 NE2 in the HL/NAG–NAG–EPO complex by corresponding direct hydrogen bonds in the HL/MAN–NAG–EPO complex (Table 3) would also not weaken the interaction. Therefore, the direct hydrogen bond between Gln104 NE2 and the O7 atom of the NAG131 residue was suggested to be a determinant for the strong recognition of the GlcNAc residue at subsite *B* in HL. The same equatorial acetylamino group exists in the MurNAc (NAM) residue, which occupies subsite *B* in the interaction between cell-wall polysaccharide and HL. The hydrogen bond might also be responsible for the substrate-recognition process in the bacteriolysis action of HL. On the other hand, a new direct hydrogen bond was plausible between the side-chain carbonyl group of Gln104 and the axial 2OH group of the mannose residue. However, this expected bond turned out to be ineffective in strengthening the interaction between the ligand and the protein. The more favourable geometry for hydrogen bonding of the 2OH group with either the adjacent 3OH group or the ring O atom at position 5 may account for the ineffectiveness.

The direct hydrogen-bonded contacts at subsite *B* involving Asp102 and Gln104 in the HL/NAG–NAG–EPO complex were also found in the HL/$(NAG)_4$–$(NAG)_2$ complex (Song *et al.*, 1994). The structurally corresponding residues to Asp102 and Gln104 in HL are Asp101 and Asn103 in HEWL and rainbow trout lysozyme (RBTL). In the HEWL/NAM–NAG–NAM complex, the MurNAc residue occupied subsite *B* and Asn103 made hydrogen bonds to the O10 and O12 atoms of the lactyl group (Strynadka & James, 1991). In the RBTL/$(NAG)_2$ complex, Asn103 ND2 made a direct hydrogen bond to the O7 atom of the GlcNAc residue at subsite *B* (Karlsen & Hough, 1995). In both complexes, Asp101 contributed by making the same hydrogen bond to the O6 atom of the residue at subsite *B*. Also, in turkey lysozyme (TEL), which replaces the Asp101 in HEWL with Gly, Asn103 is conserved and contributes to the recognition of the GlcNAc residue at subsite *B* through a pair of water-mediated hydrogen bonds to the O7 atom (Harata & Muraki, 1997). These results support the general responsibility of Gln104 (in HL) or Asn103 (in HEWL, RBTL and TEL) as well as Asp102 (in HL) or Asp101 (in HEWL and RBTL) for the substrate recognition at subsite *B* of c-type lysozymes.

The hydrophobic interaction between the apolar face of the carbohydrate residue and the aromatic plane of the side chain of the amino-acid residue results in the stacking of the two faces. The importance of such stacking interactions in substrate recognition at subsite

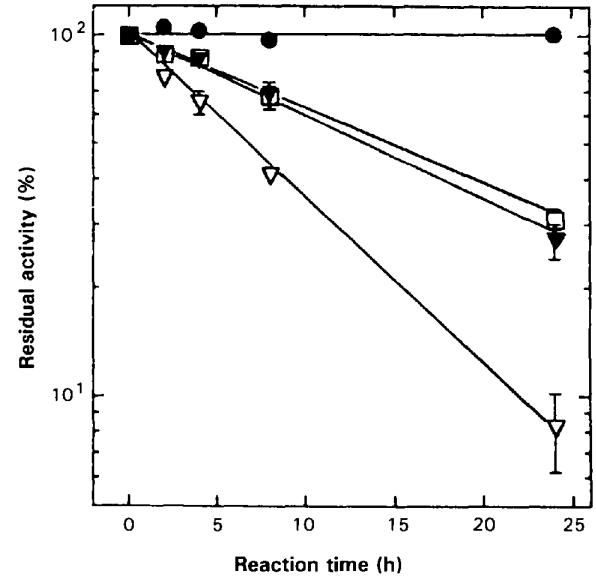

Fig. 11. Inactivation of the lytic activity of HL by affinity-labelling reagents. HL (1.0×10^{-5} *M*) was incubated with each reagent (6.6×10^{-3} *M*) at 310 K, pH 5.4. □, MAN–NAG–EPO; ▽, NAG–NAG–EPO; ▼, GAL–NAG–EPO; ●, no reagent.

B of c-type lysozymes has been pointed out for HL (Muraki *et al.*, 1992; Song *et al.*, 1994), HEWL (Strynadka & James, 1991; Cheetham *et al.*, 1992) and TEL (Harata & Muraki, 1997). The unfavourable conformation of the GAL131 residue for a stacking interaction with Tyr63 (Fig. 10), concomitant with the alteration of the hydrogen-bonded contacts (Table 3), explains well the reduced affinity of Gal-β1,4-GlcNAc compared with GlcNAc-β1,4-GlcNAc (Muraki *et al.*, 1996). In contrast, replacement of the GlcNAc residue by a Man residue did not sacrifice the parallel stacking with the side-chain group of Tyr63. An attractive C—H π-interaction has been pointed out as the origin of the stacking interaction (Nishio *et al.*, 1995). The C1—H, C3—H and C5—H bonds in both the pyranose ring of the MAN131 residue in the HL/MAN–NAG–EPO complex and the NAG131 residue in the HL/NAG–NAG–EPO complex geometrically point toward the aromatic plane of Tyr63. Although further analysis is necessary, it is possible that the C—H π-interaction contributes significantly to the parallel stacking in both complexes. In conclusion, the major cause of the decrease in affinity could be ascribed to alterations in hydrogen-bonding interactions involving Gln104. The result also suggested that the favorable conformation of the carbohydrate residue to parallel stacking with Tyr63 alone was not enough to maintain the strength of recognition at subsite *B* in HL.

This work was supported by a grant from the Agency of Industrial Science and Technology, MITI, Japan.

References

Bernstein, F. C., Koetzle, T. F., Williams, G. L. B., Meyer, E. F. Jr, Brice, M. D., Rodgers, J. R., Kennard, O., Shimanouchi, T. & Tatsumi, M. (1977). *J. Mol. Biol.* **112**, 535–542.

Blake, C. C. F., Johnson, L. N., Nair, G. A., North, A. C. T., Phillips, D. C. & Sarma, V. R. (1967). *Proc. R. Soc. London Ser. B*, **167**, 378–388.

Brünger, A. T., Kuriyan, J. & Karplus, M. (1987). *Science*, **235**, 458–460.

Cheetham, J. C., Artymiuk, P. J. & Phillips, D. C. (1992). *J. Mol. Biol.* **224**, 513–628.

Dawson, G. (1978). *Methods Enzymol.* **50**, 272–284.

Harata, K. & Muraki, M. (1997). *Acta Cryst.* D**53**, 650–657.

Jollès, P. & Jollès, J. (1984). *Mol. Cell. Biochem.* **63**, 165–189.

Jones, T. A. (1978). *J. Appl. Cryst.* **11**, 268–272.

Karlsen, S. & Hough, E. (1995). *Acta Cryst.* D**51**, 962–978.

Kraulis, P. J. (1991). *J. Appl. Cryst.* **24**, 946–950.

Laskowski, R. A., MacArthur, M. W., Moss, D. S. & Thornton, J. M. (1993). *J. Appl. Cryst.* **26**, 283–291.

Luzzati, V. (1952). *Acta Cryst.* **5**, 802–810.

Mo, F. & Jensen, L. H. (1978) *Acta Cryst.* B**34**, 1562–1569.

Moult, J., Eshdat, Y. & Sharon, N. (1973). *J. Mol. Biol.* **75**, 1–4.

Muraki, M., Harata, K., Hayashi, Y., Machida, M. & Jigami, Y. (1991). *Biochim. Biophys. Acta*, **1079**, 229–237.

Muraki, M., Harata, K. & Jigami, Y. (1992). *Biochemistry*, **31**, 9212–9219.

Muraki, M., Harata, K., Sugita, N. & Sato, K. (1996). *Biochemistry*, **35**, 13562–13567.

Nishio, M., Umezawa, Y., Hirota, M. & Takeuchi, Y. (1995). *Tetrahedron*, **51**, 8665–8701.

Quiocho, F. A. (1986). *Ann. Rev. Biochem.* **55**, 287–315.

Sato, K., Yoshimoto, A. & Takai, Y. (1997). *Bull. Chem. Soc. Jpn*, **70**, 885–890.

Sato, M., Yamamoto, M., Imada, K., Katsube, Y., Tanaka, N. & Higashi, T. (1992). *J. Appl. Cryst.* **25**, 348–357.

Song, H., Inaka, K., Maenaka, K. & Matsushima, M. (1994). *J. Mol. Biol.* **244**, 522–540.

Strynadka, N. C. J. & James, M. N. G. (1991). *J. Mol. Biol.* **220**, 401–424.

Thomas, E. W. (1970). *Carbohydr. Res.* **13**, 225–228.

Thomas, E. W., McKelvy, J. F. & Sharon, N. (1969). *Nature (London)*, **222**, 485–486.

Vyas, N. K. (1991). *Curr. Opin. Struct. Biol.* **1**, 732–740.